Enhancement of *Fusarium* head blight detection in free-falling wheat kernels using a bichromatic pulsed LED design

I-Chang Yang
National Taiwan University
Department of Bio-Industrial Mechatronics Engineering
No. 1, Section 4, Roosevelt Road
Taipei, Taiwan 106

Stephen R. Delwiche, MEMBER SPIE
United States Department of Agriculture
Agricultural Research Service
Beltsville Agricultural Research Center
Food Quality Laboratory
Building 303, BARC-East
Beltsville, Maryland 20705-2350
E-mail: stephen.delwiche@ars.usda.gov

Suming Chen
National Taiwan University
Department of Bio-Industrial Mechatronics Engineering
No. 1, Section 4, Roosevelt Road
Taipei, Taiwan 106

Y. Martin Lo
University of Maryland at College Park
Department of Nutrition and Food Science
College Park, Maryland 20742

Abstract. *Fusarium* head blight is a worldwide fungal disease of small cereal grains such as wheat that affects the yield, quality, and safety of food and feed products. The current study was implemented to develop more efficient methods for optically detecting *Fusarium*-damaged (scabby) kernels from normal (sound) wheat kernels. Through development of a high-power pulsed LED (green and red) inspection system, it was found that *Fusarium*-damaged and normal wheat kernels have different reflected energy responses. Two parameters (slope and r^2) from a regression analysis of the green and red responses were used as input parameters in linear discriminant analysis models. The examined factors affecting accuracy were the orientation of the optical probe, the color contrast between normal and *Fusarium*-damaged kernels, and the manner in which one LED's response is time-matched to the other LED. Whereas commercial high-speed optical sorters are, on average, 50% efficient at removing mold-damaged kernels, this efficiency can rise to 95% or better under more carefully controlled, kernel-at-rest conditions in the laboratory. The current research on free-falling kernels has demonstrated accuracies (>90% for wheat samples of high visual contrast) that approach those of controlled conditions, which will lead to improvements in high-speed optical sorters. © *2009 Society of Photo-Optical Instrumentation Engineers.* [DOI: 10.1117/1.3081092]

Subject terms: *Fusarium* head blight; deoxynivalenol; wheat kernel; optical sorting; mold damage.

Paper 080719R received Sep. 14, 2008; revised manuscript received Dec. 23, 2008; accepted for publication Jan. 6, 2009; published online Feb. 23, 2009.

1 Introduction

Fusarium head blight (FHB) has occurred in temperate cereal-producing regions worldwide for more than one hundred years, with its prevalence on the rise in recent years.[1] Outbreaks in North America have included those in the early 1980s, the early and mid 1990s, such as in the Midwest in 1996, and recently, the 2003 and 2004 seasons in the soft-red-winter-wheat-growing regions of the eastern United States.[2] The mycotoxin deoxynivalenol (DON), also called vomitoxin, is often produced by this mold, and causes health problems not only in livestock but also in humans. The regulation of DON in the United States is codified by the Food and Drug Administration's advisory levels for different product types and intended recipients, ranging from 1 mg/kg (human consumption), through 5 mg/kg (nonruminant animals), and up to 10 mg/kg (ruminating beef and chicken).[3] Outside the United States, many countries have similar or more stringent regulations,[4] with the European Union setting the human food limit at 0.5 mg/kg for finished products and 0.75 mg/kg for flour.[5] Aspects of food safety related to DON and tricothecenes in general are the subject of a recent review.[6]

In traditional practice, reduction of DON in grain lots is currently performed by blending with clean grain, removal of mold-damaged kernels by mechanical separation (specific gravity table), or aspiration. Advancements in the detector design and throughput rate of optical sorting devices, often used on higher-valued commodities such as pistachios, almonds, and peanuts, have led to explorations of their application to cereals such as wheat and barley, and specifically whether these devices can reduce contamination levels to within national or trade guidelines. For DON, the reduction is based on the positive, albeit imperfect, relationship between the disease's physical damage (sensitive to optical devices) and the mycotoxin level (below the measurable limit of such devices).[7]

In recent years, research has been conducted on the use of optical techniques for detection of *Fusarium*-damaged kernels (FDK, also known as scab-damaged kernels). Two broad categories of optical methods have been explored: near-infrared (NIR) spectroscopy[8] and digital image analysis. In imaging studies, kernel morphology and color characteristics are the primary features used to distinguish damaged from normal kernels.[9,10] Recognition by color is based

0091-3286/2009/$25.00 © 2009 SPIE

on the appearance of a white or pinkish color in damaged kernels. Recognition by kernel morphology is reliant on the shriveling of FDK. In recent NIR spectroscopy studies, one of the current authors (S.R.D.) has demonstrated identification of FDK in hard red winter wheat, with 95% accuracy, using two wavelengths: one in the visible region (410 to 865 nm) and the other in the NIR region (1032 to 1674 nm).[11–13] Restricting the two wavelengths to just the visible region, a less expensive option from the standpoint of sources and detectors, results in nearly 95% accuracy.

The spectrometer studies were conducted under well-controlled laboratory conditions involving diode array spectrometers and with each kernel at rest. More recent studies have looked at the potential of high-speed sorting of wheat for intrinsic properties[14,15] or disease.[16,17] An attempt to utilize an equivalent pair of wavelengths in high-speed commercial sorting resulted in an effective reduction of FDK removal efficiency to approximately 50%.[18] As a result of this diminished performance, the authors' recent studies have concentrated on alternative methods for lighting and data collection of free-falling kernels as a possible precursor to an eventual redesign of the optics for high-speed sorting. Based on a design that uses two high-power pulsed LEDs (red and green) as illumination sources, the classification accuracy for free-falling FDK has risen to approximately 72%, which is better than what was observed for commercial sorting, but shy of the accuracy experienced under controlled laboratory conditions. This has led to redesign considerations for hardware and data analysis, particularly in probe placement and signal processing. Because of the visual differences between normal and *Fusarium*-damaged kernels, it is reasoned that an increase in capture of surface-reflected light, as opposed to internally scattered light at weaker intensity, may lead to improved efficiencies in machine-based sorting systems.

The objective of the present research is to examine the improvement to FDK recognition under free-falling conditions that arise (1) from changes in the orientation of the fiber probe that receives reflected light from the kernel and (2) from a modification in the analytical procedure for relating the paired LED responses to one another, which are inherently one-half cycle out of phase. Addressing the first change, the probe angle is varied from 0 (the original setting) to 45 deg; addressing the second, LED pairing during the analysis is changed from a green-after-red (staggered) pairing to an adjusted time-equivalent basis through spline interpolation of the green LED response to the same time interval as the red LED response.

2 Experimental

2.1 *Wheat Kernel Preparation*

Wheat samples originated from a soft red winter wheat breeder's trial set that consisted of *Fusarium*-inoculated commercial releases or advanced breeders' lines. From a pool of twenty retained samples held over from an author's (S.R.D.) previous study,[19] five samples were selected for the current study. The selection process was based on visual examination of the FDK in comparison with the healthy, normal (sound) kernels within the same sample, and making a judgment as to whether the color contrast was high, moderate, or low. From the original pool, two high-contrast, two moderate-contrast, and one low-contrast samples were selected for optical tests. From each selection, kernels were drawn at random until equal numbers of 24 normal and 24 *Fusarium*-damaged kernels were obtained. These *test* kernels were stored in the wells of immunoassay trays until the time of optical examination. It is important to realize that a significant challenge for a free-falling optical system is the need to accommodate the randomness in orientation of the kernel about its long axis with respect to a viewing probe, because the only realistic degree of orientation that can be imposed on kernels exiting the chute of a commercial system would be that of the kernels' long axes.

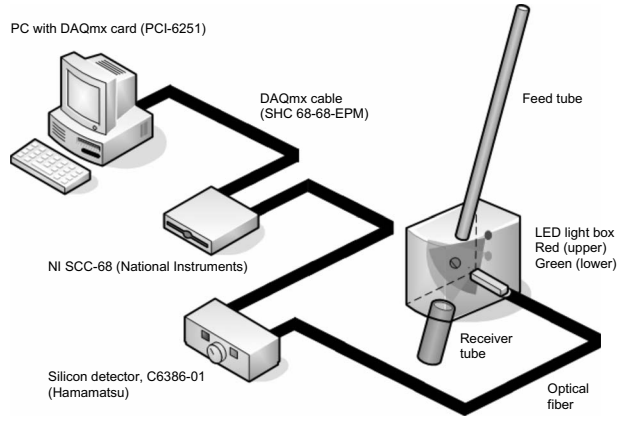

Fig. 1 Sketch of the free-falling wheat kernel inspection system (FFWKIS) apparatus.

2.2 *Experimental Apparatus and Design*

A sketch of the free-falling wheat kernel inspection system (FFWKIS) for real-time inspection is shown in Fig. 1. This device consists of a stainless steel tube (914-mm length $\times$6.3-mm i.d.) inclined at a 70-deg angle to the horizontal. The inclination angle of the tube is slightly greater than that of open-channel commercial sorters, in order to provide a greater gravitational force on the kernel to overcome the friction of the tube's interior wall, while still allowing the kernel's long axis to be coincident with the path of travel on exit from the tube. The lower end of the tube terminates within a slotted open-faced plastic electronics assembly box ($76\times67\times35$ mm) leading to an open-environment inspection region. The box, which is cut away on one end, serves two purposes: as a housing for control electronics and LEDs, and as a guide for receiving the terminal end of the feed tube. Two high-power LEDs [Luxeon I Emitters LXHL-PM01 (green, specified as $\lambda_{peak}=530$ nm, FWHM $=35$ nm) and LXHL-PD01 (red, $\lambda_{peak}=627$ nm, FWHM $=20$ nm), Phillips Lumileds Lighting Company, San Jose, Calif.] are epoxy-mounted, red above green, with a center-to-center distance of 16 mm, on a machined Bakelite card that is inserted into one of the box's slots. Previous research under controlled, kernel-at-rest conditions identified these two wavelength regions as acceptable for distinguishing FDK from sound kernels with an approximate accuracy of 95%.[13] A small stub of 12.7-mm-o.d. stainless steel tubing receives the kernel after it falls past the inspection position.

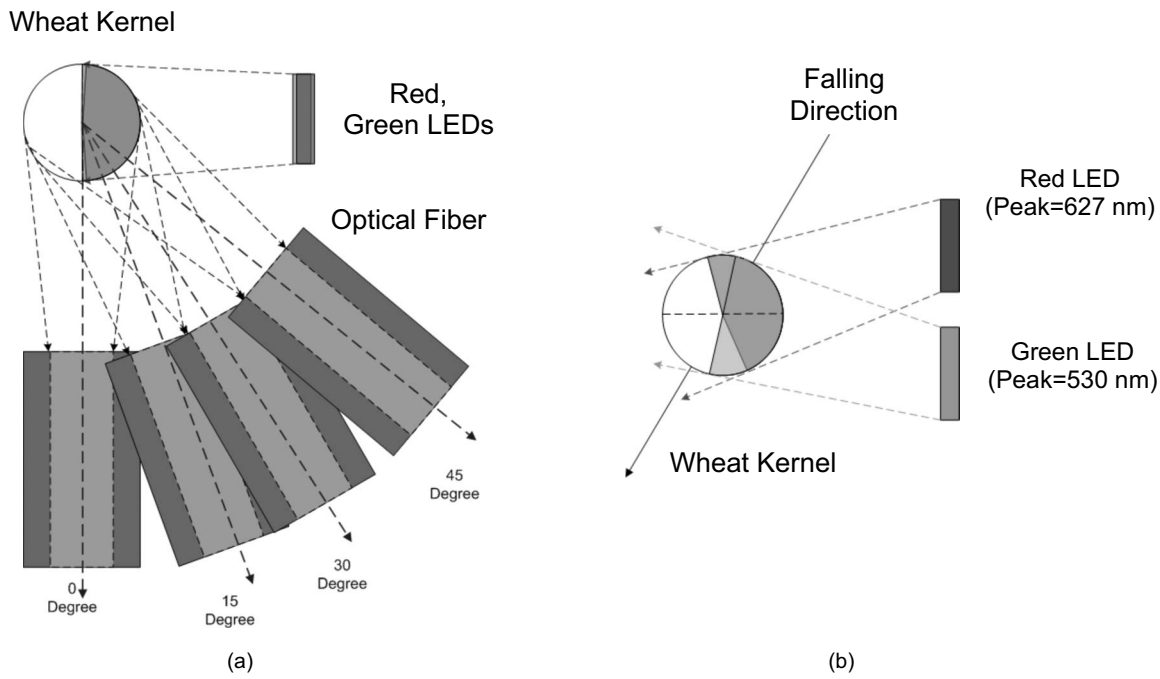

Fig. 2 Comparison of equidistant spectral measurements acquired at the four angles: (a) Top view of the wheat kernel illumination and reflectance in the FFWKIS; (b) side view of the wheat kernel illumination in the FFWKIS.

A distance of approximately 30 mm, as measured along a straight path between the feed and receiver tubes, forms the region for kernel illumination and reflectance capture by an optical fiber bundle.

The terminal end of the multifiber bundle has an internal diameter of 5 mm and is oriented in one of four angular positions (0, 15, 30, and 45 deg.) with respect to the plane of the mounting surface of the two illumination LEDs. The fixture holding the end of the bundle can be adjusted to the different angles. The opposite end of the multifiber bundle is connected by SMA connector to a silicon-detector–amplifier assembly (Hamamatsu, model C6386-01). The analog signal from this amplifier is digitized and stored by the inspection system with the use of a data grabber (NI-DAQmx PCI-6251, National Instruments), connector (NI SCC-68, National Instruments), and cable (SHC 68-68-EPM).

The inspection system originally employed LED illumination with the kernel normal to the angle of reflectance measurement by the optical fiber bundle (i.e., the 0-deg position). For the purpose of enhancing the accuracy of the system, kernel inspection was conducted using the three additional angles (15, 30, and 45 deg) of the optical fiber bundle beyond the original 0-deg position. From a top view sketch of the system [Fig. 2(a)], it can be seen that increasing the angle of the optical fiber will lead to stronger surface reflectance signal intensity. Angles greater than 45 deg were not possible because of the physical constraints of the housing. A side view sketch [Fig. 2(b)] shows that the direction of the free-falling kernel is primarily along the common centerlines of the feed and receiving tubes, so that the light from the red and green LEDs overlaps mostly on one side of the kernel.

2.3 *Operation*

A 25-ms data collection period of a 2-kHz pulse-width-modulated frequency is used for the inspection of each kernel. Each of two high-power LEDs is turned on for one half cycle, with the red and green LEDs alternating in sequence. The illumination time for an LED, which is also its rest time in the next half cycle, is 0.25 ms. In contrast with the detector sample rate of 10 per half cycle in a previous study using different hardware,[19] an 8-kHz sampling frequency was employed, which decreased the sampling rate to two per half cycle (Fig. 3). A computer program for the free-falling wheat kernel inspection system was developed in the LabVIEW environment (Version 8.2, National Instruments, Austin, TX). This single program is used to control the pulsing of the LEDs, as well as to capture the detector signal in synchronization with the LEDs. Signal acquisition is triggered by a 20-mV window trigger with 40 pretrigger data points. An algorithm was developed to determine the full width at half maximum (FWHM) of the time-domain response of reflected light from each of the two LEDs, as the kernel traverses the path of the probe's field of view. The purpose of this algorithm is to establish the baseline signal of the response detector. With baselines established,

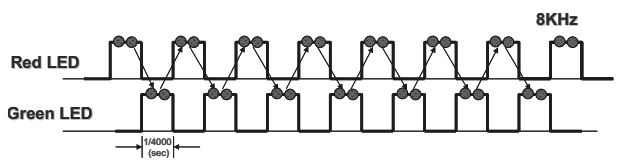

Fig. 3 The half cycles of the green and red LEDs. The gray dots represent the sampling performed by the data acquisition card.

the green LED's time-domain response is approximated by a cubic spline interpolation function, whereupon a pair of reading values is estimated for the green LED at the same instants as the two red LED responses in the preceding half cycle. This procedure is a departure from a previous study,[19] in which the green half cycle was directly paired with the preceding red half cycle, without interpolation to a common instant.

2.4 *Data Analysis*

The speed of the falling kernel was greatly influenced by the interaction of the kernel with the tube wall, such that some kernel traces demonstrated that the kernel was in the probe's field of view for a small portion of the 25-ms data collection window, while other kernels used nearly the entire window. The collection of off-baseline (>1.5 mV) response pairs of red versus green reflectance signals for each kernel was the basis for development of classifying the kernel into the normal or *Fusarium*-damaged category. From this set of paired responses for each kernel, the green light responses were linearly regressed onto the red light responses. The data reduction procedure was performed within LabVIEW immediately after data collection. The results of the regression, particularly the slope and coefficient of determination as well as the paired response readings, were stored to an external file as parameters for classification trials at a later time.

Only nonbaseline values for red- and interpolated green-LED responses were used in the regression analysis, according to the following procedure. The peak height (peak minus baseline) was separately determined for the left and right sides of the waveform. Left and right vertical heights, rather than just one height calculation, were determined for the purpose of allowing for the occasional incidence of a slanted baseline. For each height, a corresponding left or right horizontal distance (half width at half maximum, separately evaluated for each side, i.e., $\mathrm{HWHM_L}$ or $\mathrm{HWHM_R}$) was calculated. Based on trial and error, a horizontal cutoff distance of $2.2\times\mathrm{HWHM_{L\ or\ R}}$ was established for the left and right sides, and the combined central distance is referred to as FWHM. Readings lying outside of the left and right cutoffs were excluded from the regression analysis, as were points lying within the central acceptance region but less than 1.5 mV in magnitude. This procedure was implemented to enhance the reliability of the regression analysis of the waveform readings.

Based on earlier research on distinguishing normal and *Fusarium*-damaged kernels,[19] two results from the regression analysis, the slope of the line of best fit and the coefficient of determination (r^2), were examined as input parameters in a linear discriminant analysis (LDA) model. Of these two parameters, the slope was postulated to be sensitive to color differences between normal and *Fusarium*-damaged kernels. The coefficient of determination, in contrast, was postulated to be sensitive to surface textural differences between kernel classes. The classification accuracy was reported as the percentages of kernels in each category correctly classified, based on a leave-one-out cross validation. Data reduction and LDA were performed using SAS (Version 9.1, SAS Institute, Inc., Cary, NC) and its procedure DISCRIM.[20] Based on the results of these early experiments with red versus white wheat or normal versus *Fusarium*-damaged wheat, it was found that slope was the predominant classifier, with the coefficient of determination adding only a marginal improvement. However, with changes to both hardware and the data reduction procedure in the current study, it was considered important to retain r^2, in addition to the slope, in the initial classification trials. After the slope was again determined to be the predominant classifier (see Secs. 3 and 4), the analysis focused on this parameter alone.

For the slope parameter, two clustering procedures were used. The first procedure involved the systematic trial of values for a slope threshold, choosing a value between 0 and 1 in increments of 0.001, and then determining the number of normal and *Fusarium*-damaged kernels lying on opposite sides of the threshold. From this stepwise search, the optimal threshold was determined for each sample of 24 normal and 24 *Fusarium*-damaged kernels. The second procedure was similar to an earlier study involving LDA,[19] this time with resubstitution only (i.e., no cross validation because of similarity of findings—see Secs. 3 and 4). The slope threshold procedure serves as an upper bound to the accuracies that can be obtained from the LDA procedure. Programming of the first procedure was performed in MATLAB 6.5 (The Mathworks, Inc., Natick, MA); the second procedure was performed in the SAS procedure DISCRIM. The results from the regression analysis were also analyzed using MATLAB 6.5 to calculate the optimal threshold of the slope without r^2. Analyses of variance were performed on both procedures, in which the total percentage of correctly classified kernels was tested with probe angle as the main factor and contrast group as a blocking factor. Comparisons of means were performed using Duncan's multiple range test.

3 Results

3.1 *Signal Acquisition*

Figure 4 shows an example of all the kernel responses for one of the trays in the high-contrast set, inspected at one measurement angle (45 deg) and subsequently displayed in the MATLAB environment. The odd-numbered samples are the normal kernels, and the even-numbered samples are the *Fusarium*-damaged kernels. Generally, the traces of the normal kernels tend to display a narrower and higher Gaussian-shaped time response than those of the FDK, which produce lower and wider responses. The narrower waveform is indicative of a higher speed during free fall caused by the greater mass of normal kernels, which results in a smaller influence of air resistance. Because the kernel is inspected in free fall, having first tumbled through the feed tube, it is not possible to precisely align the kernel about its long axis. Visual inspection of these traces reveals that inherent differences between normal and *Fusarium*-damaged kernels are overshadowed by variability associated with the randomness of orientation of a kernel during free fall. Therefore, it is advantageous for classification algorithms to be uninfluenced by the rotational position of the kernel.

As a means to demonstrate the parameterization procedure, the reflectance curves for a typical normal kernel and FDK are shown in Fig. 5(a). Images of these two kernels

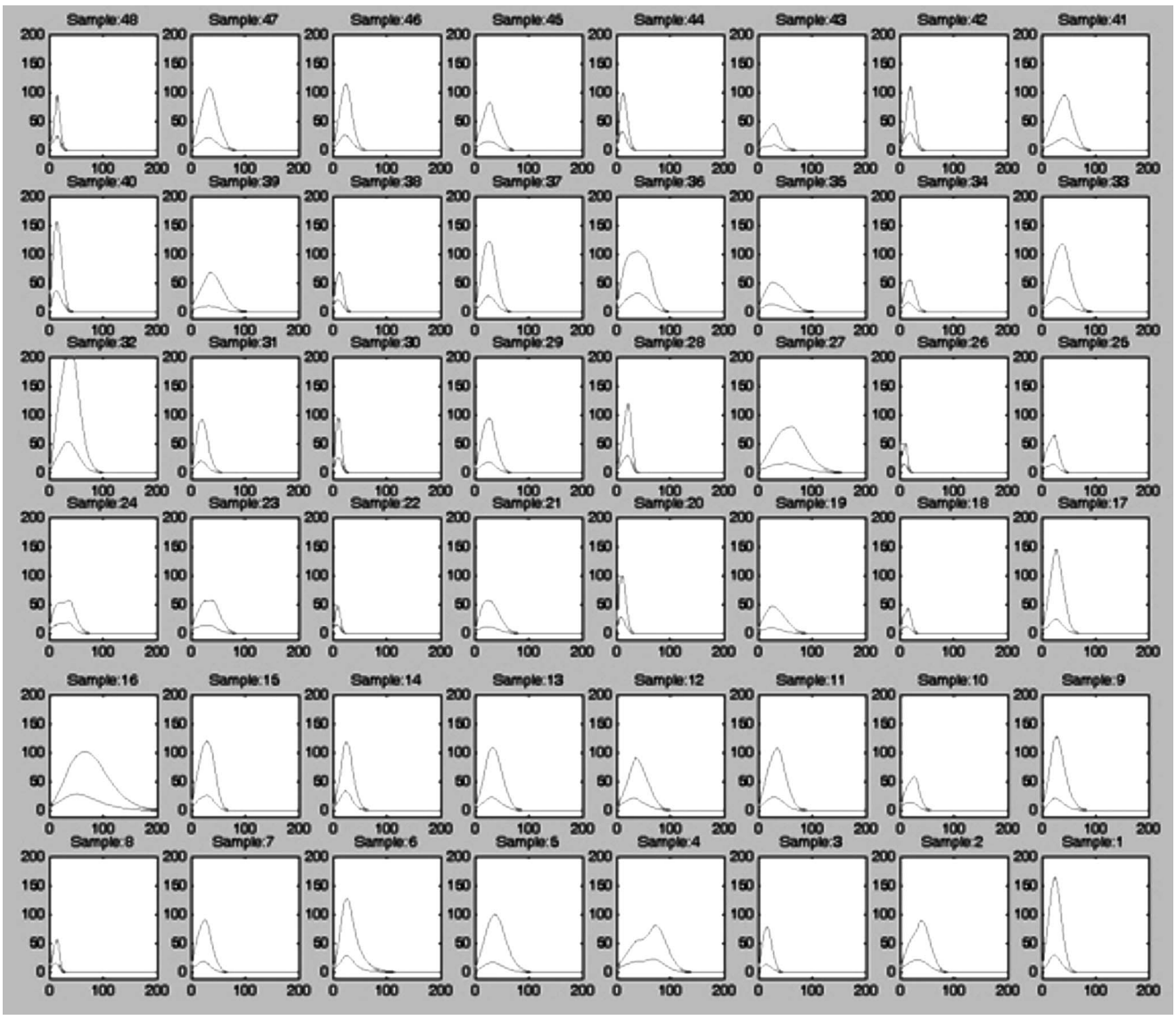

Fig. 4 The reflectance response curves of 48 kernels in one tray. The curves of the kernels in high-contrast set 1, inspected with a 45-deg optic fiber angle, are shown as an example.

are contained inside the graph. On implementing the FWHM procedure outlined earlier for each side of each reflectance curve, plots of the qualifying (i.e., >1.5 mV) detector responses, processed by a green-onto-red spline interpolation scheme, are shown in Fig. 5(b). For each kernel, the best fit line is shown, recalling that it is the slope (Δ green LED/Δ red LED) and corresponding r^2 that are used in the classification analysis.

3.2 *Angle and Analysis Methods*

The schematic of Fig. 2(a) shows the illuminated areas of the kernel covered by the four different probe angles. The intensity of the reflected energy from the kernel was greatly affected by the probe angle. Whereas the peak response of the red LED was typically 50 to 100 mV when the probe angle was 0 deg, this value rose to approximately 250 mV at the 45-deg angle. The green LED response, always smaller than the red LED response, also increased as the angle increased from 0 to 45 deg.

Because of the random interaction of the kernel and feed tube wall, the kernel was readily affected by the frictional forces within the tube, so that its exit speed and rotational position were also variable. Therefore, the r^2 value varied highly in both *Fusarium*-damaged and normal situations. LDA trials (not shown) that utilized both slope and r^2 as classification parameters failed to reveal any added benefit of the latter parameter. Thus, it was surmised that the effect of the randomness of kernel orientation on reflected energy was sufficiently large to overshadow any effect that might have been attributed to surface texture differences between normal and *Fusarium*-damaged kernels. This can be seen by the graphical example of one high-contrast sample (2H) measured three times (Fig. 6). The trend of higher slope

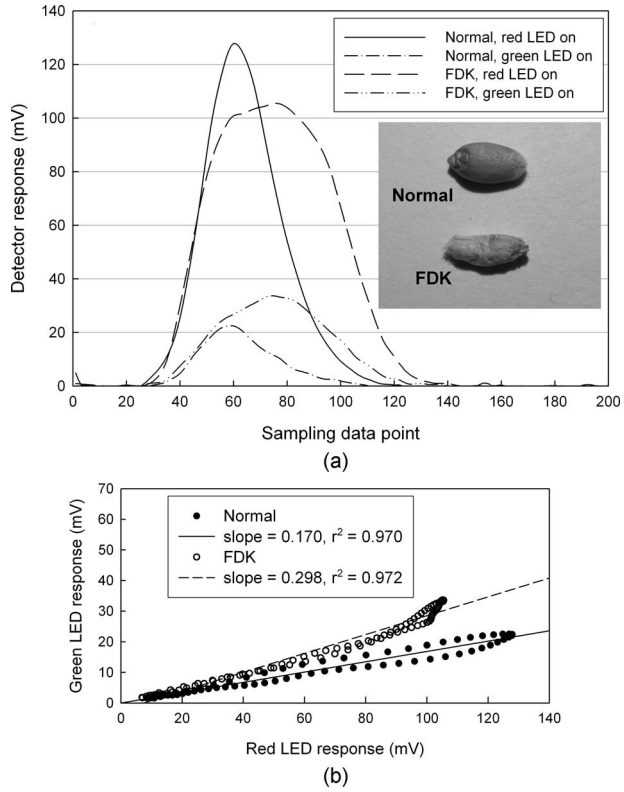

Fig. 5 The instrument response and data processing of a representative normal kernel and a *Fusarium*-damaged kernel (FDK) selected from high-contrast set 1, 45-deg probe angle: (a) the spline-interpolated reflected energy readings during red- and green-LED illumination; (b) the results of the green-onto-red linear regression analyses for these two kernels, inclusive of the slopes and coefficient of determinations that are subsequently used in classification.

values for FDK is apparent, but there is still a large amount of variation attributable to random orientation, as seen by the nonoverlapping of the triplicate readings for slope and r^2. Again, separation of normal and *Fusarium*-damaged kernels along the horizontal (r^2) axis is not apparent. For this reason, only the slope was used in the subsequent cluster analyses.

Using the slope parameter in LDA, the classification results, defined as the percentage of correctly identified kernels after resubstitution of each kernel's reading into the LDA model, are shown in Table 1. The best total result, at 91.67%, was for the 2H set under the 45-deg condition, with 21 of 24 and 23 of 24 *Fusarium*-damaged and normal kernels correctly classified, respectively. The corresponding cross-validation (based on a one-kernel-out per rotation cycle design) accuracies for this set were the same as the resubstitution accuracies, which was also true for 17 of the 19 other contrast-set$\times$angle conditions. Because of the similarity in resubstitution and cross-validation accuracies, the latter values are hereafter not reported. Using the 1H $\times$45-deg set as an example, a plot of slope versus r^2 for the 24 *Fusarium*-damaged and 24 normal kernels of this sample is shown in Fig. 7, in which 24 and 20 correct classifications were respectively on the correct side of the threshold, yielding a total accuracy of 91.67%. The corresponding total accuracy for the LDA was 87.50%. The results of the optimal slope threshold calculation for all sets are shown in Table 2, which is arranged in the same manner as the LDA results of Table 1.

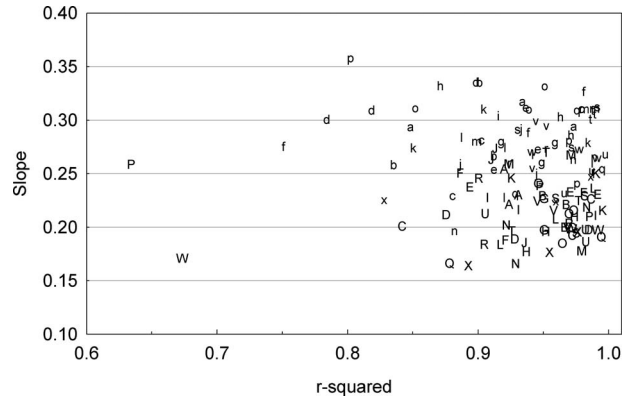

Fig. 6 Repeated measurements on one sample (high-contrast set 2, 45-deg probe angle), consisting of 24 normal kernels and 24 *Fusarium*-damaged kernels. Each kernel was measured three times and is identified by a unique alphabetical character, with normal kernels in UPPERCASE and *Fusarium*-damaged kernels in lowercase.

Both Table 1 (LDA results) and Table 2 (thresholding) show the effect of probe angle on the classification accuracy. For either procedure, the 45-deg probe angle was significantly different ($P<0.05$) than the 0-deg angle, with the 15- and 30-deg-angle accuracies lying between the two extremes. This finding is indicative of the benefit of positioning the probe at an oblique angle to the illumination path, as opposed to the 0-deg angle used in previous free-falling studies.

3.3 *Contrast of Kernels*

The contrast levels of the different kernel sets were selected by visual observation, with subjective criteria and without prior instrumental analysis. Compared to the two sets of

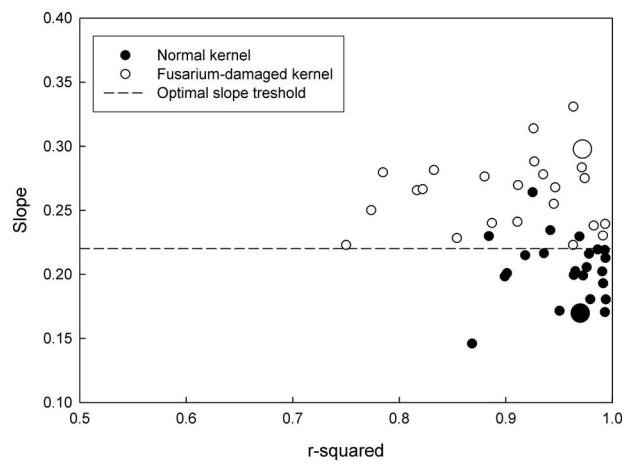

Fig. 7 The optimal threshold for separating normal and *Fusarium*-damaged kernels of one tray (high-contrast set 1) at a 45-deg fiber probe angle. The two enlarged symbols correspond to the kernels depicted in Fig. 5.

Table 1 Results of linear discriminant analysis for all measurement angles and contrast sets. Nonsignificant differences among the average values for the total percentage correct at the four angles are indicated by a common letter (P=0.05) in the rightmost column.

Angle (deg)	Contrast level	Correctly identified scab		Correctly identified normal		Total correct		Set
		Out of 24	(%)	Out of 24	(%)	Out of 48	(%)	
0	1H	19	79.17	18	75.00	37	77.08	a
	1L	16	66.67	16	66.67	32	66.67	
	1M	15	62.50	16	66.67	31	64.58	
	2H	17	70.83	19	79.17	36	75.00	
	2M	18	75.00	19	79.17	37	77.08	
15	1H	20	83.33	20	83.33	40	83.33	ab
	1L	15	62.50	18	75.00	33	68.75	
	1M	19	79.17	24	100.00	43	89.58	
	2H	18	75.00	20	83.33	38	79.17	
	2M	18	75.00	21	87.50	39	81.25	
30	1H	20	83.33	21	87.50	41	85.42	ab
	1L	17	70.83	20	83.33	37	77.08	
	1M	16	66.67	18	75.00	34	70.83	
	2H	19	79.17	22	91.67	41	85.42	
	2M	17	70.83	17	70.83	34	70.83	
45	1H	20	83.33	22	91.67	42	87.50	b
	1L	18	75.00	22	91.67	40	83.33	
	1M	19	79.17	19	79.17	38	79.17	
	2H	21	87.50	23	95.83	44	91.67	
	2M	21	87.50	20	83.83	41	85.42	

high contrast, the intermediate-contrast sets had fewer highly noticeable damaged kernels, and the low-contrast set had only subtle visual differences between normal and *Fusarium*-damaged kernels. There were no apparent differences in overall kernel size (length or width) among the five samples. When averaged across angular position, the two high-contrast sets produced higher accuracies than the other sets. The accuracies of both high-contrast sets could exceed 90% in different analysis methods. For the effect of angle and contrast, the results at 15 and 30 deg are variable with intermediate-contrast sets (Fig. 8).

3.4 *Method of Pairing LED Responses*

The two methods (staggered and spline interpolation) of pairing the LED response readings that were used to determine the slope of the relationship between the two LEDs are compared for the probe angle of 45 deg in Fig. 9. The total percentages of correctly classified kernels from the resubstitution of the LDA function for each method are plotted for each contrast set. In four of the five sets, the spline interpolation method was superior to the staggered method. In the fifth set (moderate contrast), the classification rate was equal between the two methods. For the three other probe angle positions (not shown), the spline interpolation method was superior in all contrast sets.

4 Discussion

Previous studies reported that color, rather than texture, as sensed by the free-falling kernel apparatus, was the dominant classifier. This finding was reaffirmed in the current study, in that the coefficient of determination offered no significant contribution as a classifier. The two new findings of this study are both encouraging from the standpoint of improving the accuracy of recognition of FDK in free

Table 2 Results of the optimal threshold method for all measurement angles and contrast sets. Nonsignificant differences among the average values for the total percent correct at the four angles are indicated by a common letter (P=0.05) in the rightmost column.

Angle (deg)	Contrast level	Slope threshold	Correctly identified scab		Correctly identified normal		Total correct		Set
			Out of 24	(%)	Out of 24	(%)	Out of 48	(%)	
0	1H	0.249	20	83.33	18	75.00	38	79.17	a
	1L	0.305	13	54.17	21	87.50	34	70.83	
	1M	0.262	16	66.67	15	62.50	31	64.58	
	2H	0.269	17	70.83	20	83.33	37	77.08	
	2M	0.269	18	75.00	19	79.17	37	77.08	
15	1H	0.271	21	87.50	20	83.33	41	85.42	ac
	1L	0.303	14	58.33	21	87.50	35	72.92	
	1M	0.267	19	79.17	24	100.00	43	89.58	
	2H	0.264	21	87.50	20	83.33	41	85.42	
	2M	0.257	23	95.83	19	79.17	42	87.50	
30	1H	0.250	20	83.33	21	87.50	41	85.42	ab
	1L	0.233	22	91.67	18	75.00	40	83.33	
	1M	0.250	17	70.83	18	75.00	35	72.95	
	2H	0.246	19	79.17	23	95.83	42	87.50	
	2M	0.263	17	70.83	18	75.00	35	72.92	
45	1H	0.220	24	100.00	20	83.33	44	91.67	c
	1L	0.240	20	83.33	22	93.67	42	87.50	
	1M	0.242	21	87.50	18	75.00	39	81.25	
	2H	0.223	23	95.83	22	91.67	45	93.75	
	2M	0.246	20	83.33	22	93.67	42	87.50	

fall. The first finding is that placement of the probe at an oblique angle, such as 45 deg, enhances the reflected energy signal of both red and green LEDs, but more important, it also improves the ability to distinguish normal and *Fusarium*-damaged kernels, as demonstrated by an increase in average accuracy from 72.1% (0 deg) to 85.4% (45 deg) for LDA (Table 1) and from 73.8% (0 deg) to 88.3% (45 deg) for threshold analysis (Table 2). When the system was initially designed, the placement of the probe at the 0-deg position was made for the purpose of reducing the contribution of surface reflectance relative to diffuse reflectance. Contrary to this original thought that the diffuse component would be more useful in separating normal and damaged kernels, it appears that the opposite idea is true—that surface color, rather than any underlying property, is the best parameter for identifying FDK. Although probe

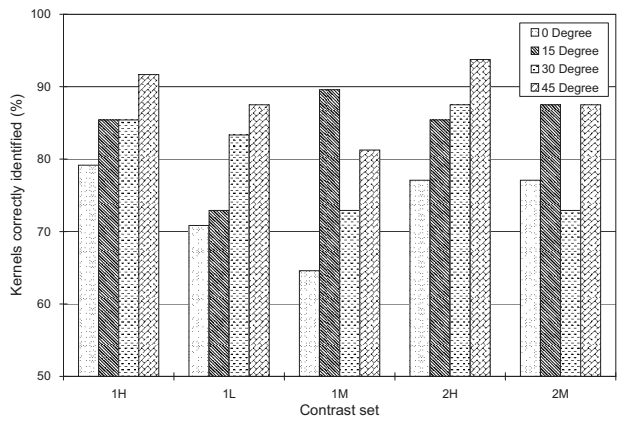

Fig. 8 Kernels correctly classified using the optimal slope threshold determined for each angle at each contrast set.

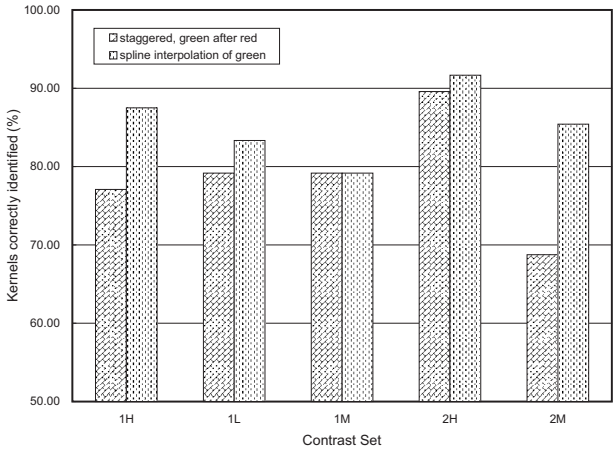

Fig. 9 Comparison of the method of LED response pairing in linear discriminant analysis using the green-onto-red slope as the classification parameter, at the 45-deg probe position. The two methods refer to the manner in which the green response is paired with the red response (staggered=green half cycle response paired to preceding red half cycle; spline interpolation of green=green responses adjusted by spline interpolation to time instances of red responses).

angles greater than 45 deg were not examined because of physical constraints of the system, it is possible that additional improvements in accuracy may be gained at greater angles. This will be a topic of future research.

The second finding is that it is advantageous to adjust one of the LED responses (green was selected for this study) to the same time window as the other LED. A two-LED, one-detector system requires the raw signal responses to be one-half cycle out of phase. The earlier assumption that a 0.25-ms phase imbalance would be inconsequential to the classification models does not appear to be true. Instead, interpolation, either by a cubic spline function (reported herein) or a simple linear interpolation (also tested but not reported), is beneficial to improving classification. This is because the regression analysis that relates the two LED responses is more accurately representing the responses to a common time basis, which was found to be critical in the use of slope as a classification parameter.

Lastly, while the bulk of this study concentrated on the clustering of kernel responses one sample at a time, the effect of angle when all five samples are pooled together was also explored (Fig. 10). Again, the benefit of the oblique probe angle is apparent, with the 45-deg angle demonstrating an optimal slope threshold level that correctly

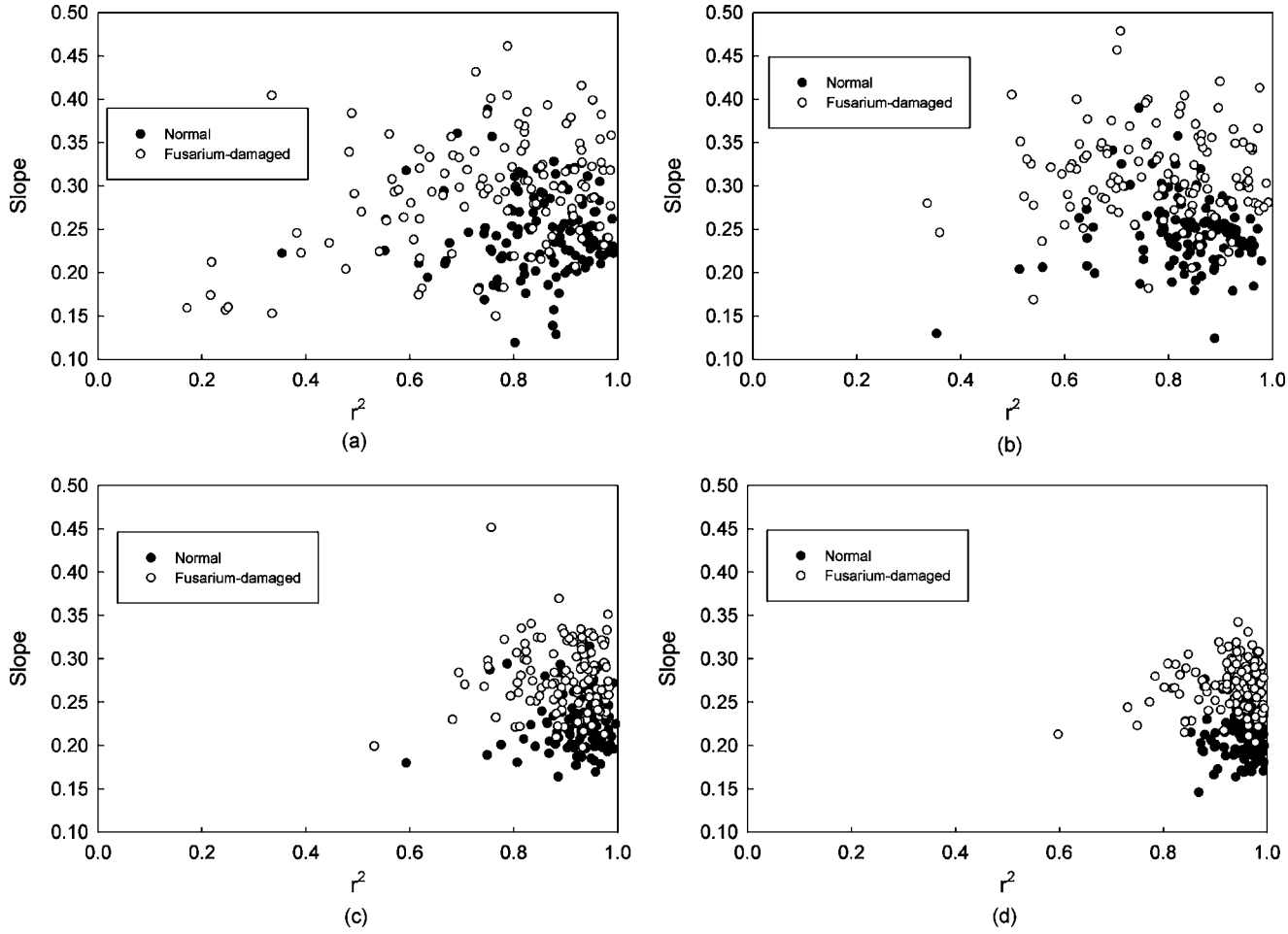

Fig. 10 The r^2 and slope distribution for kernel samples of all contrast sets combined, and the optimal threshold for the combined set, for probe angles of (a) 0, (b) 15, (c) 30, and (d) 45 deg.

Table 3 Results of optimal slope threshold method for the four measurement angles.

Angle (deg)	Contrast level	Slope threshold	Correctly identified scab		Correctly identified normal		Total correct	
			Out of 120	(%)	Out of 120	(%)	Out of 240	(%)
0	Optimal threshold	0.271	82	68.33	91	75.88	173	72.08
15		0.266	103	85.83	94	78.33	197	82.08
30		0.251	92	76.67	96	80.00	188	78.33
45		0.236	104	86.67	101	84.17	205	85.42

categorizes 85.4% of the kernels (Table 3), as compared with a low of 72.1% accuracy for the 0-deg setting.

5 Summary and Conclusions

The accuracy of the free-falling wheat kernel inspection system was enhanced by modifying the optical structure and the data analysis method. The angular position of the optical fiber with respect to the free-falling kernel and LED light source was modified to allow for acquisition of more reflected energy from the kernel. Of the three new angles examined (15, 30, and 45 deg), the best result was obtained at 45 deg. A spline interpolation was also used to simulate the simultaneous response of red and green reflectances instead of the raw staggered configuration. The slope of the red and green regression function continued to be of greater utility as a classification parameter than the coefficient of determination. The best discrimination result of any single tray was 93.75%, and the best discriminant result of all trays combined was 85.42%.

Acknowledgment

The authors thank Professor Carl Griffey, Department Crop and Soil Environmental Sciences, Virginia Polytechnic Institute and State University, who contributed the wheat samples.

References

1. R. W. Stack, "History of *Fusarium* head blight with emphasis on North America," Chap. 1 in *Fusarium Head Blight of Wheat and Barley*, K. J. Leonard and W. R. Bushnell, Eds., pp. 1–34, The American Phytopathological Society, St. Paul, MN (2003).
2. L. P. Hart, "Variability of vomitoxin in truckloads of wheat in a wheat scab epidemic year," *Plant Dis.* **82**, 625–630 (1998).
3. U.S. Food and Drug Administration "Letter from Ronald Chesemore to State Agricultural Directors, state feed control officials, and food, feed and grain trade organizations on advisory levels for DON (vomitoxin) in food and feed U.S. Department of Health and Human Services," Public Health Service, Rockville, MD (1993).
4. FAO, "Worldwide regulations for mycotoxins in food and feed in 2003," in *Food Nutr. (Roma)* p. 81, Food and Agriculture Organization of the United Nations, Rome (2003).
5. Codex, "Discussion paper on deoxynivalenol. Codex Committee on Food Additives and Contaminants," in *35th Session, Codex Alimentarius Commission*, FAO/WHO, Rome (2003).
6. J. E. Dexter and T. W. Nowicki, "Safety assurance and quality assurance issues associated with *Fusarium* head blight in wheat," Chap. 16 in *Fusarium Head Blight of Wheat and Barley*, K. J. Leonard and W. R. Bushnell, Eds., pp. 420–460, Am. Phytopathological Soc., St. Paul, MN (2003).
7. P. A. Paul, P. E. Lipps, and L. V. Madden, "Relationship between visual estimates of *Fusarium* head blight intensity and deoxynivalenol accumulation in harvested wheat grain: a meta-analysis," *Phytopathology* **95**, 1225–1236 (2005).
8. F. E. Dowell, M. S. Ram, and L. M. Seitz, "Predicting scab, vomitoxin, and ergosterol in single wheat kernels using near-infrared spectroscopy," *Cereal Chem.* **76**, 573–576 (1999).
9. X. Luo, D. S. Jayas, and S. J. Symons, "Identification of damaged kernels in wheat using a colour machine vision system," *J. Cereal Sci.* **30**, 49–59 (1999).
10. R. Ruan, S. Ning, A. Song, A. Ning, R. Jones, and P. Chen, "Estimation of *Fusarium* scab in wheat using machine vision and a neural network," *Cereal Chem.* **75**, 455–459 (1998).
11. S. R. Delwiche, "Classification of scab- and other mold-damaged wheat kernels by near-infrared reflectance spectroscopy," *Trans. ASAE* **46**, 731–738 (2003).
12. S. R. Delwiche and G. A. Hareland, "Detection of scab damaged hard red spring wheat kernels by near-infrared reflectance," *Cereal Chem.* **81**, 643–649 (2004).
13. S. R. Delwiche and C. S. Gaines, "Wavelength selection for monochromatic and bichromatic sorting of *Fusarium*-damaged wheat," *Appl. Eng. Agric.* **21**, 681–688 (2005).
14. M. C. Pasikatan and F. E. Dowell, "Evaluation of a high-speed color sorter for segregation of red and white wheat," *Appl. Eng. Agric.* **19**, 33–38 (2003).
15. M. C. Pasikatan and F. E. Dowell, "High-speed NIR segregation of high- and low-protein single wheat seeds," *Cereal Chem.* **81**, 145–150 (2004).
16. F. E. Dowell, T. N. Boratynski, R. E. Ykema, A. K. Dowdy and R. T. Staten, "Use of optical sorting to detect wheat kernels infected with *Tilletia indica*," *Plant Dis.* **86**, 1011–1013 (2002).
17. T. C. Pearson, D. T. Wicklow, and M. C. Pasikatan, "Reduction of aflatoxin and fumonisin contamination in yellow corn by high-speed dual wavelength sorting," *Cereal Chem.* **81**, 490–498 (2004).
18. S. R. Delwiche, T. C. Pearson, and D. L. Brabec, "High-speed optical sorting of soft wheat for reduction of deoxynivalenol," *Plant Dis.* **89**, 1214–1219 (2005).
19. S. R. Delwiche, "High-speed bichromatic inspection of wheat kernels for mold and color class using high-power pulsed LEDs," *Sensing Instrum. Food Quality Safety* **1**(2), 103–110 (2008).
20. SAS Institute Inc., "The DISCRIM procedure," Chap. 25 in *SAS/STAT® 9.1 User's Guide*, pp. 1137–1246, SAS Institute Inc., Cary, NC (2004).

I-Chang Yang is a PhD candidate in the Department of Bio-Industrial Mechatronics Engineering at National Taiwan University. He was an exchange student at the University of Maryland, College Park, from 2007 to 2008, and also was a visiting scholar in the Food Safety Lab, USDA Beltsville Agricultural Research Center, Beltsville, MD, in the same period. His area of specialization includes the technology of nondestructive sensing of biomaterials, remote sensing, precision agriculture, multispectral imaging, hyperspectral imaging, and spectral chemometric analysis.

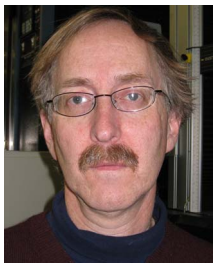

Stephen R. Delwiche is an agricultural engineer employed by the USDA Agricultural Research Service in Beltsville, MD, where he has worked since 1990. His area of specialization includes the development of optical devices and procedures for rapid and (ideally) nondestructive analysis of small grains for food quality and safety, addressing the needs of commerce, processors, and official inspection operations. Dr. Delwiche serves on the editorial board of *Cereal Chemistry* and is past chair of the Engineering and Processing Division of the American Association of Cereal Chemists. He is active in SPIE, ASABE, AACC International, and the Council for Near Infrared Spectroscopy.

Suming Chen is a professor in the Department of Bio-Industrial Mechatronics Engineering and the director of the Bioenergy Research Center at National Taiwan University. Dr. Chen is editor-in-chief of the *Journal of Agricultural Machinery* (JAM) and is also vice editor-in-chief of *Engineering in Agriculture, Environment and Food* (EAEF). His areas of specialization include nondestructive sensing of biomaterials, remote sensing and precision agriculture, automation in agriculture, renewable energy, and computer simulation and control.

Y. Martin Lo, associate professor of food bioprocess engineering and director of the Food Science Graduate Program at the University of Maryland, is the editor-in-chief of the *Journal of Food Processing and Preservation*. He has also served on the graduate faculty of the Bioengineering Department. Dr. Lo is recognized for his extensive experience in the development of novel food-processing and preservation technologies. He has established active research programs in value-added applications of food and agriculture by-products as well as development of processing technologies to enhance food safety. Dr. Lo is the U.S. Department of Agriculture (USDA) Food Safety Inspection Services (FSIS) HACCP coordinator for the State of Maryland and served as the 2006–2007 chair of the Institute of Food Technologists (IFT) Food Engineering Division. An initial member of the UM NanoCenter, Dr. Lo was honored as the 2007–2009 Distinguished Lecturer by the IFT, amongst other recognitions.